THE JOURNAL OF PHYSICAL CHEMISTRY B

Article

pubs.acs.org/JPCB

Dynamic Phase Diagram of a Nonionic Surfactant Lamellar Phase

Luigi Gentile,*[,†,‡] Manja A. Behrens,[‡] Sandor Balog,[§,∥] Kell Mortensen,[⊥] Giuseppe A. Ranieri,[†] and Ulf Olsson[‡]

[†]Dipartimento di Chimica e Tecnologie Chimiche, University of Calabria, P. Bucci 14C, 87036 Rende, Italy

[‡]Division of Physical Chemistry, Department of Chemistry, Lund University, P.O. Box 124, SE-221 00 Lund, Sweden

[§]Laboratory for Neutron Scattering, Paul Scherrer Institut, 5232 Villigen PSI, Switzerland

[∥]Adolphe Merkle Institute, University of Fribourg, 1723 Marly 1, Switzerland

[⊥]Niels Bohr Institute, University of Copenhagen, 2100 Copenhagen, Denmark

ABSTRACT: The dynamic phase diagram of triethylene glycol dodecyl ether ($C_{12}E_3$) in D_2O was determined for 40, 50, and 60 wt % of surfactant. The shear flow effect on the nonionic lamellar phase was investigated as a function of temperature and concentration. The transition from planar lamellae (L_α)-to-multilamellar vesicles (MLVs) was characterized by means of rheology, rheo-small-angle neutron and light scattering. New insight into the nature of the transition region between L_α and the MLVs state is provided. A disorder−order transition was also observed by SANS. This is attributed to a transition from disordered MLVs to a close-packed array of MLV's with slightly higher order than before. Moreover flow instability was observed in the shear-thickening regime at 40 °C.

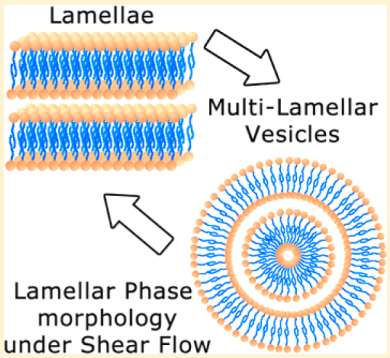

1. INTRODUCTION

Systems prone to shear-induced structural changes are interesting and fascinating. These systems can have significant impact on industrial pipeline processing, for instance, viscosity issues during the extrusion process. Dramatic changes in the viscosity, which is often associated with structural rearrangement of the system, can give rise to shear-thinning or shear-thickening behavior.[1−15] For these reasons, the equilibrium phase diagram is not sufficient to describe these types of chemical systems; in fact, the nonequilibrium state are also relevant. Thus dynamic phase diagrams should be investigated.

In many cases, the lamellar phases exhibit a strong nonlinear response due to the bilayer bending rigidity and relative spontaneous curvature.[2−15] The formation of multilamellar vesicles (MLVs so-called onions) from planar lamellae has been observed in these types of systems. The MLV formation results in a considerable increase in viscosity. Several authors propose that the coupling of short-wavelength thermal undulations with strain deformation leads to a coherent stripe buckling of the lamellae that eventually results in MLV formation.[16] However, it has been proposed that shear-induced MLVs can result from the occurrence of lamellar phase defects, expected to exist in these systems, which can relax external and internal stresses.[17−19]

The presence of MLV can be unambiguously identified by combining rheology with nuclear magnetic resonance (NMR), small-angle light, and X-ray or neutron scattering (SALS, SAXS, and SANS). Rheo-tools applied in situ have been used to perform deformation experiments in combination with several techniques: NMR, microscopy, SALS, SAXS, and SANS.

Nonionic polyoxyethylene alkyl ether surfactants (C_nE_m) are relatively simple molecules known to exhibit a variety of phases in aqueous solution, as a function of temperature and concentration. C_nE_m/water systems strongly respond to deformation stimuli. The results obtained in the past years on these systems are quite interesting: using flow-SANS and rheo-SALS, Zipfel et al.[20] have identified the multilamellar cylinders (MLCs) as the intermediate state between planar lamellae and MLVs in the $C_{10}E_3/D_2O$ system. Le et al.[21] have observed a closely packed honeycomb-shaped MLV state in the $C_{12}E_4/D_2O$ system. In this case, the MLVs are hexagonally packed into layers that slide relative to each other under shear flow, and the corresponding two-dimensional (2D) SANS and SAXS scattering patterns show hexagonal symmetries.[22,23] Moreover, using rheo-SALS experiments, Suganuma et al.[22] showed the existence of MLV packed in a hexagonal shape in the $C_{12}E_4/D_2O$ system. Usually, the presence of onions is indicated by a four-lobe cloverleaf SALS pattern.

Banding phenomena were reported for $C_{16}E_4$[24,25] and $C_{10}E_3$.[26] These shear and vorticity banding phenomena were studied by flow-SANS and flow-NMR, respectively. Furthermore, viscosity oscillations were observed for $C_{16}E_4$ due to a variation of the MLV fraction in the bulk.

Flow curves are used to construct the dynamic phase diagrams of C_nE_m surfactants in water.[14,27] Usually, the shear rate ($\dot{\gamma}$) dependence of the viscosity (η) has been divided into

Received: January 28, 2014
Revised: March 10, 2014
Published: March 11, 2014

three zones when MLV formation is present. First at lower shear rate, a shear-thinning regime is present (zone 1). This regime corresponds to the orientation or alignment of the lamellar phase in the flow direction. Increasing the shear rate, shear-thickening appears (zone 2) due to the MLV formation. At high shear rates (zone 3) shear-thinning behavior is again found probably due to densely packed-MLVs as suggested by Fujii and Richtering,[28] and the relationship between viscosity and shear rate can be described by a power law.

The MLV formation was observed at 34 °C for 50 wt % of $C_{12}E_3$ in D_2O.[14] A minimum shear rate of 1 s^{-1} was required to obtain the MLV formation, and by exceeding this value, the process appears to be strain-controlled. The transition from planar lamellae to MLVs follows a path similar to that reported for the $C_{10}E_3/D_2O$ system at 40 wt %, requiring a slightly lower strain.[23,27]

In this paper, results concerning the influence of shear deformation on the $C_{12}E_3/D_2O$ system for concentrations between 40 and 60 wt % and at temperatures between 24 and 40 °C are presented. A better understanding of the temperature-dependent behavior is obtained by a rheological study of 50 wt % of $C_{12}E_3$ in D_2O as a function of shear rate. To correlate the macroscopic rheological behavior with the microstructure evolution, in situ SANS and SALS experiments of the system under shear were performed. The dynamic phase diagrams are constructed for three concentrations of surfactant using the experimental results mainly coming from rheology. Moreover, the MLVs in the densely packed state are discovered and a rheo-chaos regime is identified providing new insight into flow-behavior effects that are not yet fully understood. The main focus here is on concentration- and temperature-dependence in the MLV formation.

2. MATERIALS AND METHODS

2.1. Materials. Triethylene glycol dodecyl ether ($C_{12}E_3$) was purchased from Nikko Chemicals Co., Ltd. (Tokyo, Japan). Deuterium oxide (D_2O) was purchased from Armar Chemicals. The purity of each material is higher than 99.8%, and the materials were used without further purification. The samples were prepared by mixing the surfactant and D_2O. The mixing was assisted by gentle stirring, and the mixtures were left overnight.

The $C_{12}E_3$/water phase diagram is similar to that of the $C_{10}E_3$/water system.[29] The lamellar phase (L_α) is stable in the temperature range between 20 and 50 °C and present over a broad range of concentrations.

2.2. Rheology. Measurements were carried out using a shear-stress-controlled rheometer, Physica UDS 200 (Anton Paar, Germany) equipped with a Couette cylinder geometry (inner diameter of 25 mm and a gap of 1 mm). The temperature was controlled by a water circulator apparatus (±0.2 °C). To prevent any evaporation, measuring geometries were surrounded by a solvent trap containing water.

Transient experiments (nonlinear rheology) were performed by step-rate tests in the range between 0.1 and 100 s^{-1}. The macroscopic shear rate ($\dot{\gamma}$) is defined as the ratio between the velocity over the gap, and the shear stress is defined as the macroscopic force divided by the surface. Under steady shear, non-Newtonian fluids exhibit a variety of nonlinear responses, including yield stress, shear thinning, and shear thickening. For a wide variety of shear-thinning or shear-thickening fluids, a power law can adequately describe the relationship between viscosity and shear rate

$$\eta \propto \dot{\gamma}^{(n-1)} \tag{1}$$

where η is the apparent viscosity also called transient or shear viscosity. For a Newtonian liquid $n = 1$, while for shear-thinning and shear-thickening liquids $n > 1$ and $n < 1$, respectively.

2.3. Rheo-SALS. Small-angle light scattering (SALS) experiments were performed using an Anton Paar Physica MCR 301 rheometer equipped with a glass cone−plate geometry with a diameter of 43 mm and a cone angle of 2°. For all measurements, a 10 mW diode laser operating at a wavelength of 658 nm was used as the light source. Scattering patterns from depolarized light were captured using a CCD camera (Lumenera Corporation, Ottawa, Canada) located below the screen. The depolarized patterns were collected with crossed polarizer and analyzer. The primary beam was parallel to the velocity-gradient direction, and the scattering pattern was detected in the plane defined by the shear flow and vorticity (neutral) direction (Figure 1).

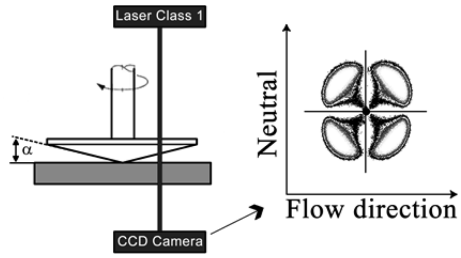

Figure 1. Schematic diagram of the rheo-SALS for the cone−plate setup.

2.4. Flow-SANS. Small-angle neutron scattering (SANS) experiments were performed on the SANS-II beamline at the Swiss Spallation Neutron Source (SINQ) at the Paul Scherrer Institute, Switzerland.[30] The sample was held in a Couette cell with an inner rotating cylinder of 29 mm diameter and a gap equal to 1 mm. The measurements were performed at a shear rate of 2, 5, 10, and 60 s^{-1} and performed in the temperature range between 24 and 42 °C. The neutron beam traversed the shear-cell radially, through the cylinder centers (i.e., the scattering is observed in the plane expanded by the flow and the neutral directions perpendicular to the shear gradient) (Figure 2).[31]

The neutron wavelength was 6.02 Å, and the sample-to-detector distance was 1.2 m, covering a q range of 0.027−0.24 $Å^{-1}$. The raw data were corrected for empty cell scattering and put to an absolute scale by calibration with incoherent water

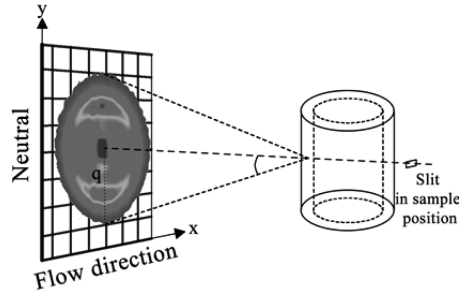

Figure 2. Schematic diagram of the flow-SANS setup in the radial configuration: velocity gradient (z axis), shear flow direction (x axis), and neutral vorticity (y axis).

dx.doi.org/10.1021/jp5009797 | J. Phys. Chem. B 2014, 118, 3622−3629

scattering. In the flow-SANS experiments, evaporation was avoided by using a sealed Couette.

3. RESULTS AND DISCUSSION

3.1. Rheological Results: Flow Curves. The steady-state viscosity (η) and shear stress (σ) are shown in Figure 3 as a function of the shear rate ($\dot{\gamma}$) ranging from 0.1−100 s^{-1}, for a 50 wt % solution of $C_{12}E_3$ in D_2O at temperatures of 24 and 40 °C. Three regimes are indicated on the flow curve at 24 °C shown together with SALS patterns (Figure 1A) focusing on the viscosity behavior; the first regime is almost a plateau, while a slight increase in viscosity is observed at $\dot{\gamma}$ of 2 s^{-1}. This may indicate a second regime, which is a transition regime ascribed to the formation of MLV, however small, at 24 °C. The SALS pattern recorded in the first regime confirm the presence of the planar lamellae (L_α) in agreement with previous results on the $C_{10}E_3/D_2O$ system,[32] while the pattern recorded in the second regime indicates the presence of defects in the texture as already discussed in the literature.[2] In fact, the pattern is characterized by a rather diffuse intensity distribution with slightly enhanced scattering intensity along and perpendicular to the flow direction. However, the presence of a few MLVs cannot be excluded; a mixture of MLVs and L_α is reported for $C_{10}E_3$.[23] The nature and presence of this transition zone is still unclear, and further investigations are required. The third regime clearly shows shear-thinning behavior, and this can be well-described by a power law relation $\eta \propto \dot{\gamma}^{-0.6\pm0.1}$, while looking at the shear stress, the power law observed is $\sigma \propto \dot{\gamma}^{-0.4\pm0.1}$. The structure factor peak appearing in the SALS pattern recorded in this regime confirms the presence of MLVs. The reader should consider that the SALS pattern at 0.5 s^{-1} is recorded after around 10000 strain units, while 20000 and 120000 are the strain units of the patterns recorded at 2 and 60 s^{-1}, respectively. The flow curve at 40 °C appears to be similar to the one observed at 34 °C,[14] but with a larger and more distinct second regime than that observed at 24 °C. The first regime, at low shear rates, shows a shear-thinning type behavior, which is expected to originate from orientation or alignment of the lamellar phase in the flow direction. The second regime, from 1 to 10 s^{-1}, shows a shear-thickening-type behavior associated with the MLV formation. This shear-thickening regime is identified as a transition zone that in this case is attributed to a coexistence of MLVs and planar lamellae.[23,24,33] The third regime, at high shear rates, shows a shear-thinning type behavior like that of regime one. It can be described by the following power laws $\eta \propto \dot{\gamma}^{-0.67\pm0.01}$ and $\sigma \propto \dot{\gamma}^{-0.33\pm0.01}$. The shear-thinning exponents are comparable to those obtained for other systems over a similar range of shear rates. An exponent of −0.8 was observed for a variety of systems, including an SDS-based system as reported by Roux et al.,[34] an AOT-based system reported by Bergenholtz and Wagner,[33] and $C_{16}E_4/D_2O$ as reported by Gentile et al.[24] On the other hand, in an AOT-based system at high surfactant concentration[35] and in a $C_{10}E_3/D_2O$ system,[27] shear-thinning exponents equal to −0.5 were observed. The shear-thinning regime is associated with densely packed-MLVs.[28] Dissimilarities in the slope may be related to differences in the densely packed structures; however, one should also consider diverse experimental conditions. In any case, the results suggest formation of a closely packed MLV state, which in our case is at higher shear rates. Rheological data for 40 wt % were qualitatively similar to a 50 wt % sample, while 60 wt % has a planar lamellae viscosity behavior except at high shear flow and low temperature, as confirmed by SANS data (see Concentration Dependence of MLV Formation).

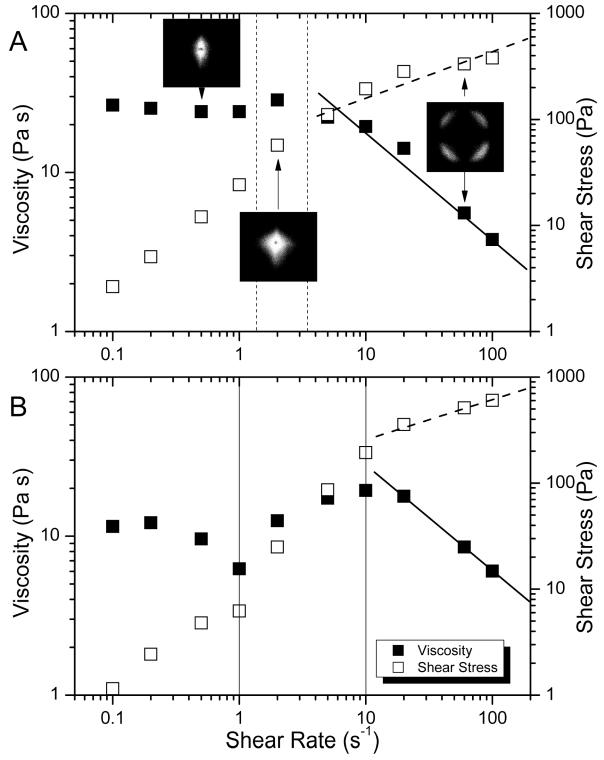

Figure 3. Steady-state shear stress (□) and viscosity (■) as a function of the shear rate at (A) 24 °C and (B) 40 °C. Rheological data were obtained after transient experiments at fixed shear rates in the steady state for 50 wt % of $C_{12}E_3$ in D_2O. The solid and dashed lines each show a power law relation, while the vertical lines are guides for the eyes, separating the three different regions. The SALS patterns reported at 24 °C are obtained at 0.5, 2, and 60 s^{-1} after 1×10^4, 2×10^4, and 12×10^4 strain units, respectively.

3.2. Concentration Dependence of MLV Formation. Figure 4 shows the behavior of the 2D SANS patterns as a function of temperature for $C_{12}E_3/D_2O$ under shear rate of 10 and 60 s^{-1} for (a) 40 wt % and (b) 60 wt % of the surfactant. The following observations are made for the system at 40 wt %: (i) SANS patterns are not completely isotropic as one expects for MLVs, instead a slight anisotropy is observable, (ii) the scattering intensity of the patterns recorded at 60 s^{-1} is higher than at 10 s^{-1}. The behavior of the two-dimensional (2D) SANS patterns of $C_{12}E_3/D_2O$ with a surfactant concentration of 60 wt % is shown in Figure 2B as a function of temperature. Here the following observations can be made: (i) at a shear rate of 10 s^{-1}, no changes are observed in the L_α patterns, (ii) MLVs appear only at 24 °C and 60 s^{-1}. If the surfactant concentration is increased, MLVs are not likely to form. The absence of MLVs was observed in other systems as well.[19,36] This result confirms the double dependence of the MLV formation by bending and saddle-splay moduli.[24] The bending modulus is strictly related to the d spacing and as consequence to the surfactant concentration.[37] Moreover the d spacing of the lamellar phase at 40 wt % is 6.5 ± 0.2 nm in the range between 24 and 40 °C at 10 s^{-1}, while it becomes 5.7 ± 0.2 nm when increasing the shear rate at 60 s^{-1}. The d spacing at 60 wt % of the surfactant is 4.7 ± 0.2 nm for all temperatures and for both

dx.doi.org/10.1021/jp5009797 | J. Phys. Chem. B 2014, 118, 3622−3629

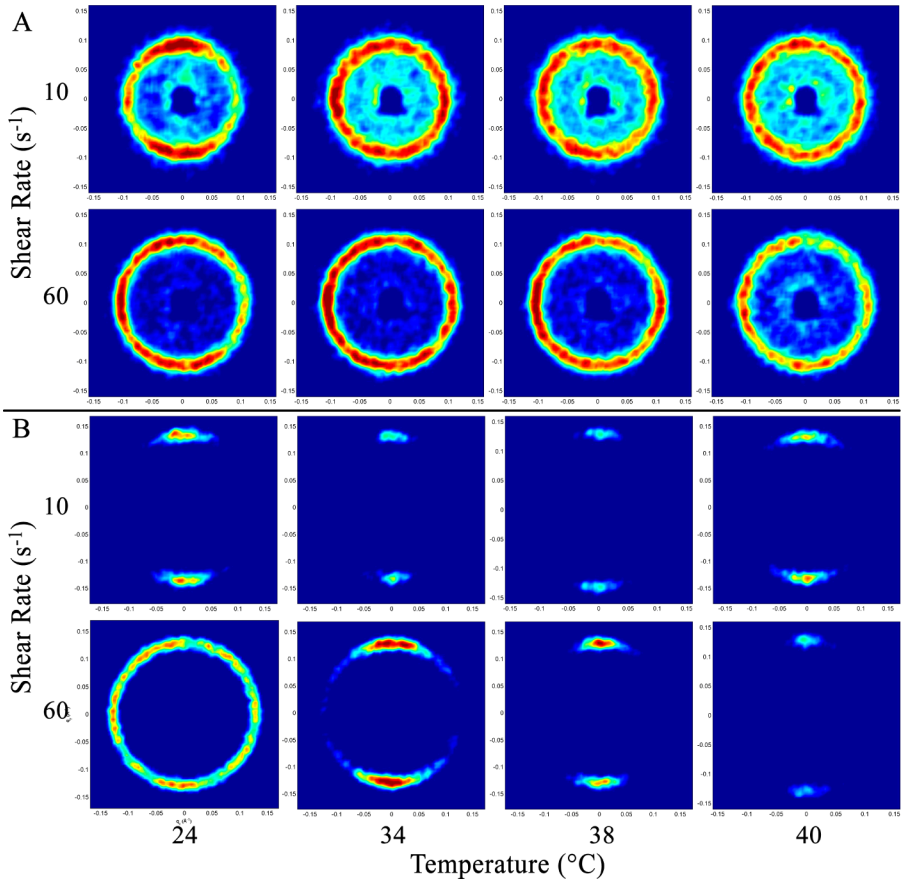

Figure 4. Steady-state scattering patterns as a function of temperature and shear rate for (A) 40 wt % and (B) 60 wt % of $C_{12}E_3$ in D_2O.

shear rates. These evidence confirm the strong relationship between concentration and bending modulus.

3.3. Dynamic Phase Diagram. The morphological behavior of the lamellar phase under the shear flow was investigated using rheology, SALS, and SANS techniques. Rheology was used to examine changing in the bulk parameters (i.e., viscosity), with SALS to get the averaged shape and size of MLVs on the micrometer scale and SANS in order to reveal changes to the lamellar membranes on the nanometer scale. The experimental results are summarized in the dynamic phase diagrams in Figure 5, where the steady-state structure is shown in temperature-shear rate space for three surfactant concentrations.

The dynamic phase diagrams presented in Figure 5 are mainly constructed using steady-state viscosities, as reported previously for the $C_{10}E_3/D_2O$ system.[27]

3.3.1. Small-Angle Light Scattering Probe. The depolarized 2D SALS patterns at a shear rate of 60 s^{-1} for $C_{12}E_3$ at 40 and 50 wt % shows a four-lobe structure factor at 34 °C, while at 24 °C, the form factor is observed at 40 wt % of surfactant (Figure 6). The vesicles are closely packed at $\dot{\gamma}$ of 60 s^{-1} (Figure 3), and therefore, the observed SALS pattern is affected by interparticle diffraction. In this state, the MLVs can be measured from the position of the intensity maximum. Accordingly, eq 2 was used to estimate the approximate MLV size:[14,36]

$$q_{max} = \frac{3.9}{R_{MLV}} \quad (2)$$

where q_{max} corresponds to the q value where the scattered intensity reaches its maximum. In the case of the form factor,

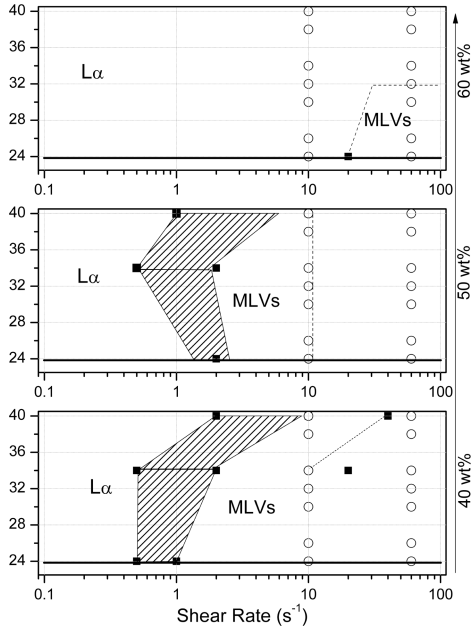

Figure 5. Dynamic phase diagrams in the temperature-shear rate space for three surfactant concentrations in D_2O. ○ represent measured points using SANS or SALS, while ■ represent measure points using rheology. Nevertheless, not all rheological data are shown. The dashed part indicates the intermediate transition zone. The MLVs at high shear rates for 40 and 50 wt % of surfactant have a slightly higher order than the MLVs obtained at low shear rates (see Ordered MLV).

dx.doi.org/10.1021/jp5009797 | J. Phys. Chem. B 2014, 118, 3622−3629

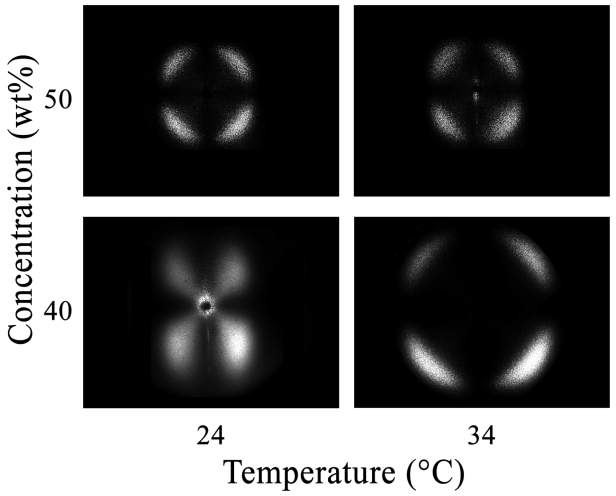

Figure 6. 2D SALS patterns recorded for 40 and 50 wt % of $C_{12}E_3$ in D_2O at shear rate of 60 s^{-1} and a temperature of 24 and 34 °C. All patterns were obtained in the steady state at about 12 × 10^4 strain units.

the following equation was used $q_{max} = 4.1/R_{MLV}$.[14,36] R_{MLV} are 0.9 ± 0.2 and 0.8 ± 0.1 μm at 24 °C and are 0.5 ± 0.1 and 0.8 ± 0.1 μm at 34 °C for 40 and 50 wt % of surfactant, respectively. The sizes are in partial agreement with the data reported in literature;[14] however, the patterns reported here are recorded at higher strain units than previously reported. The results indicate the absence of temperature effects on the MLV size at high concentration, while at 40 wt %, the size changes with temperature due mainly to the hexagonally densely packed MLV state at 34 °C. An MLV size jump in temperature for the $C_{12}E_4/D_2O$ system was also reported by Suganuma et al.,[22] while an increase of the MLV size with increasing temperature was reported for $C_{16}E_7/D_2O$.[36] This may be due to the coupled relation between MLV size with lamellar elasticity and temperature. Further investigation of the MLV size dependence in these kinds of systems is needed.

3.3.2. Ordered MLV. The disorder−order transitions in the MLV phase are caused by the polydisperse-monodisperse transition according to Suganuma et al.[22] Griffith et al.[38] showed that the disordered hard spheres with the size polydispersity of 7% still have a definite structure factor peak at the volume fraction of 0.5. Therefore, the structure factor peak observed in the previous SALS pattern likely reflects disordered MLVs with polydisperse MLV size. On the other hand the disorder−order transition of the MLVs might take place with a small change in the polydispersity. SANS experiments were performed in order to investigate the structural morphology of the steady state. The SANS pattern reveals an almost hexagonal arrangement of bilayers in the velocity−vorticity plane. Small-angle light scattering experiments on the related $C_{12}E_4$/water system has demonstrated that this state corresponds to a densely packed MLV state with the onions forming hexagonally packed layers in the velocity−vorticity plane. Figure 7A shows the azimuthal intensity distribution of the SANS pattern recorded in the steady state at $\dot{\gamma}$ of 10 s^{-1}.

The presence of the MLVs is established by correlating data from SANS, rheological, and SALS (Rheological Results: Flow Curves and Concentration Dependence of MLV Formation). The SANS pattern changes from the almost isotropic ring to a

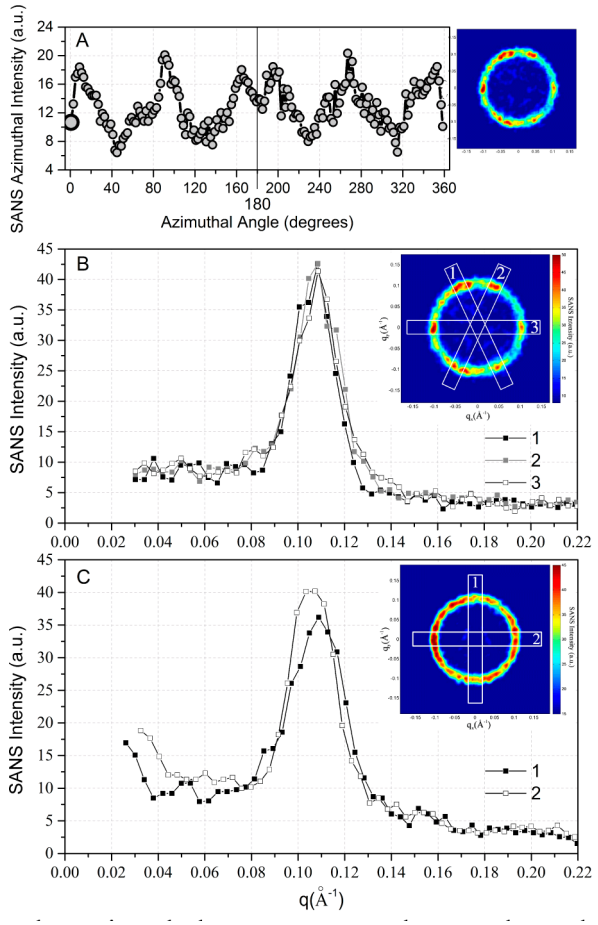

Figure 7. (A) Azimuthal trace averaged around a q band 0.06−0.16 $Å^{-1}$ of the SANS pattern under a shear rate of 10 s^{-1} recorded at about 8 × 10^4 strain units in the steady state at 24 °C for 50 wt % of $C_{12}E_3$. SANS profiles along the selected directions under a shear rate of 10 s^{-1} at (B) 24 °C and (C) 34 °C in the steady state for 50 wt % of $C_{12}E_3$ in D_2O.

six-spot pattern at about 8 × 10^4 strain units, which is related to changes in the phase texture.

Figure 7 (panels B and C) reveal minor differences between the two states comparing the scattering curves in the neutral and flow directions at 34 °C and in the six spot directions at 24 °C. The larger intensity difference in the neutral-flow plane for 34 °C indicates elongation in the flow field and that the MLVs at higher temperature are more susceptible to flow than the more organized structure. This demonstrates a disorder−order transition of the MLV packing. The q-dependent peak-widths, reflecting the multilamellar order, remains unchanged within experimental accuracy, showing that the lamellar correlations are both affected by MLV-ordering.

Note that the azimuthal trace in the ordered phase has a nonequivalent intensity distribution with the peak positions at about 8°, 92°, 164°, 196°, 268°, and 352°, indicating an elastic deformation of ordered MLVs due to the applied shear, though the q position of the six spots is always the same at ∼0.11 $Å^{-1}$.

Similar results were obtained for the $C_{12}E_4/D_2O$ system at 40 wt %.[3,23] However, a higher symmetry of the hexagonal pattern was observed for $C_{12}E_4$, and as a consequence, the close-packed arrays of MLVs for $C_{12}E_3$ have a lower order than for $C_{12}E_4$.

Hexagonal packing has only been observed in C_nE_m/water systems for $C_{12}E_4$ and for $C_{12}E_3$, as reported here. The L_α to

dx.doi.org/10.1021/jp5009797 | J. Phys. Chem. B 2014, 118, 3622−3629

MLV transition under shear flow is mainly related to the saddle-splay modulus, $\bar{\kappa}_m$, of the bilayer;[39] that is,[40]

$$\bar{\kappa} = 2\bar{\kappa}_m - \delta K\beta(T - T_0) \quad (3)$$

where $\bar{\kappa}$ is the monolayer saddle-splay modulus, δ is the bilayer thickness, κ is the bending modulus, and $\beta(T - T_0) \approx H_0(T)$ is the monolayer spontaneous curvature term. H_0 is the term most affected by temperature,[40] and this is why MLV formation is temperature-dependent.[36] A similar explanation can be given for the hexagonal packing MLV state. In other C_nE_m/water systems, one can also relate the absence of the hexagonal packing at comparable strain units to the bending modulus. In fact, two main structural properties significantly influence the bending rigidity, κ, in the Würger model:[41] the hydrophobic chain length and the polar head surface area of the surfactant.

3.4. Flow Instabilities. Experiments have shown both sustained and erratic temporal viscosity oscillations in surfactant mesophases and solutions,[42−46] particularly in $C_{16}E_4/D_2O$.[47] Chaotic behavior of bulk flow at virtually zero Reynold's number must stem from nonlinearity, as expressed in the rheological constitutive equation and has been called 'rheochaos'.[48−50] There are some indications that these erratic signals result from deterministic chaotic dynamics.[2,43,48−51] The unstable temporal viscosity behavior, in the case of $C_{16}E_4$, was due to the variation of the fraction of two lamellae states: MLVs and classic lamellar phase. In fact, these structural aggregations have a different resistance to flow. A fraction of planar lamellae changes in MLVs upon time and vice versa. Viscosity oscillations in 50 wt % of $C_{12}E_3$ were observed at 40 °C at shear rates of 2 and 5 s^{-1} (Figure 8).

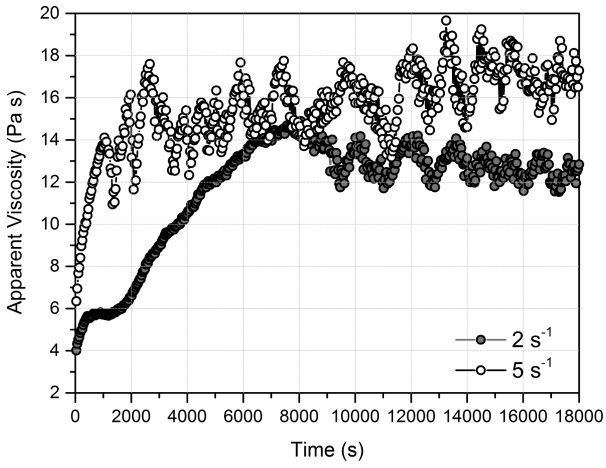

Figure 8. Evolutions of the apparent viscosity at 2 and 5 s^{-1} of 50% $C_{12}E_3$, as obtained at 40 °C.

However, the rheological data does not correspond to the flow-SANS data, as the erratic viscosity signal is not strictly correlated with the SANS intensities. On the other hand, it should be noted that the rheological and flow-SANS data are recorded separately. The viscosity oscillations are probably due to structural oscillations between planar lamellar and vesicles that determines the transition zone reported in Figure 5.

4. CONCLUSIONS

In this paper, new insights into the nature of the transition zone in the dynamic phase diagram were reported. The intermediate transition zone between planar lamellae and MLVs can be related (i) to the increase of defects in the lamellar phase as previously reported,[1] (ii) to the coexistence between planar lamellae and MLVs,[23,24,33] or (iii) to structural oscillations between planar lamellar and vesicles.[47] Our rheo-SALS data confirms the increase of defects in the lamellar phase at 24 °C, while flow instabilities appear when the temperature is increased to 40 °C, due to variations in the fraction MLVs relative to the planar lamellae in the $C_{12}E_3/D_2O$ system. These results raise the following questions concerning the oscillatory state. (i) Is the oscillatory state a common step for all systems that show transitions under shear flow? (ii) Are the oscillations related strictly to the induced structure? To answer these questions, systematic investigations of several systems should be performed.

The experimental results presented here were successfully used for the first time to determine the dynamic phase diagram of the $C_{12}E_3/D_2O$ system. This type of phase diagram is a powerful tool to predict steady-state structures under shear as a function of temperature and composition. Here MLVs are found in the temperature range between 24 and 40 °C of the lamellar phase starting with a shear rate of 2 s^{-1} for 40 and 50 wt % of surfactant. MLVs appear only at high shear rate (i.e. 60 s^{-1}) and at a temperature of 24 °C for the system at 60 wt %. The hexagonally densely packed MLV state was observed by SANS, though with a lesser degree of order than previously shown for the $C_{12}E_4/D_2O$ system. From the rheo-SALS experiments, performed at the shear rate of 60 s^{-1}, the average radius of the MLVs was determined at different temperatures and concentrations. No temperature dependence of the MLVs size was observed at 50 wt % of the surfactant, while at 40 wt %, smaller MLVs were observed at high temperature. This temperature dependence is mainly due to the transition from a dilute MLVs state to a densely packed state.

AUTHOR INFORMATION

Corresponding Author

*E-mail: luigi.gentile@unical.it. Tel: +390984493385.

Notes

The authors declare no competing financial interest.

ACKNOWLEDGMENTS

We thank the Paul Scherrer Institute for access to the SANS-II beamline of SINQ (proposal: 20111446). Moreover, we thank the Knut and Alice Wallenberg Foundation for supporting the purchase of the rheo-SALS instrument. S.B. is grateful for the financial support of the Adolphe Merkle Foundation. M.B. acknowledges the Villum Kann Rasmussen foundation for financial support. K.M. thanks DANSCATT for support. U.O. thanks the Swedish Research Council for financial support. The authors acknowledge financial support from the European Commission under the Seventh Framework Program by means of the grant agreement for the Integrated Infrastructure Initiative N. 262348 European Soft Matter Infrastructure (ESMI). This paper is also cofinanced by the European Commission, European Social Fund, and the Region of Calabria. The authors are solely responsible for this paper, and the European Commission and the Region of Calabria are not responsible for any use that may be made of the information contained therein.

REFERENCES

(1) Angelico, R.; Burgemeister, D.; Ceglie, A.; Olsson, U.; Palazzo, G.; Schmidt, C. Deuterium NMR Study of Slow Relaxation Dynamics in a Polymer-like Micelles System after Flow-Induced Orientation. *J. Phys. Chem. B* **2003**, *107*, 10325−10328.

(2) Diat, O.; Roux, D.; Nallet, F. Effect of Shear on a Lyotropic Lamellar Phase. *J. Phys. II* **1993**, *3*, 1427−1452.

(3) Müller, S.; Börschig, C.; Gronski, W.; Schmidt, C. Shear-Induced States of Orientation of the Lamellar Phase of $C_{12}E_4$/Water. *Langmuir* **1999**, *15*, 7558−7564.

(4) Medronho, B.; Rodrigues, M.; Miguel, M. G.; Olsson, U.; Schmidt, C. Shear-Induced Defect Formation in a Nonionic Lamellar Phase. *Langmuir* **2010**, *26*, 11304−11313.

(5) Lu, C. Y. D.; Chen, P.; Ishii, Y.; Komura, S.; Kato, T. Non-linear Rheology of Lamellar Liquid Crystals. *Eur. Phys. J. E* **2008**, *25*, 91−101.

(6) Fritz, G.; Wagner, N. J.; Kaler, E. W. Formation of Multilamellar Vesicles by Oscillatory Shear. *Langmuir* **2003**, *19*, 8709−8714.

(7) Wunenburger, A. S.; Colin, A.; Leng, J.; Arnéodo, A.; Roux, D. Oscillating Viscosity in a Lyotropic Lamellar Phase under Shear Flow. *Phys. Rev. Lett.* **2001**, *86*, 1374−1377.

(8) Sato, D.; Obara, K.; Kawabata, Y.; Iwahashi, M.; Kato, T. Re-Entrant Lamellar/Onion Transition with Varying Temperature under Shear Flow. *Langmuir* **2013**, *29*, 121−132.

(9) Bergmeier, M.; Gradzielski, M.; Hoffmann, H.; Mortensen, K. Behavior of Ionically Charged Lamellar Systems under the Influence of a Shear Field. *J. Phys. Chem. B* **1999**, *103*, 1605−1617.

(10) López-Barrón, C. R.; Basavaraj, M. G.; DeRita, L.; Wagner, N. J. Sponge-to-Lamellar Transition in a Double-Tail Cationic Surfactant/Protic Ionic Liquid System: Structural and Rheological Analysis. *J. Phys. Chem. B* **2012**, *116*, 813−822.

(11) Fischer, P.; Schmidt, C.; Finkelmann, H. Amphiphilic Liquid-Crystalline Networks: Phase Behavior and Alignment by Mechanical Fields. *Macromol. Rapid Commun.* **1995**, *16*, 435−447.

(12) Le, T. D.; Olsson, U.; Mortensen, K. Topological Transformation of a Surfactant Bilayer. *Phys. B* **2000**, *276*, 379−380.

(13) Le, T. D.; Olsson, U.; Mortensen, K.; Zipfel, J.; Richtering, W. Nonionic Amphiphilic Bilayer Structures under Shear. *Langmuir* **2001**, *17*, 999−1008.

(14) Gentile, L.; Rossi, C. O.; Olsson, U. Rheological and Rheo-SALS Investigation of the Multi-Lamellar Vesicle Formation in the $C_{12}E_3/D_2O$ System. *J. Colloid Interface Sci.* **2012**, *367*, 537−539.

(15) Gentile, L.; Rossi, C. O.; Olsson, U.; Ranieri, G. A. Effect of Shear Rates on the MLV Formation and MLV Stability Region in the $C_{12}E_5/D_2O$ System: Rheology and Rheo-NMR and Rheo-SANS Experiments. *Langmuir* **2011**, *27*, 2088−2092.

(16) Zilman, A.; Granek, R. Undulation Instability of Lamellar Phases under Shear: A Mechanism for Onion Formation? *Eur. Phys. J. B* **1999**, *11*, 593−608.

(17) Medronho, B.; Miguel, M. G.; Olsson, U. Viscoelasticity of a Nonionic Lamellar Phase. *Langmuir* **2007**, *23*, 5270−5274.

(18) Dhez, O.; Nallet, F.; Diat, O. Influence of Screw Dislocations on the Orientation of a Sheared Lamellar Phase. *Europhys. Lett.* **2001**, *55*, 821.

(19) Fujii, S.; Isojima, T.; Sasaki, N.; Kubota, K.; Nakata, M. Shear-Induced Structural Transformation of Pentaethylene Glycol n-Dodecyl Ether and Lithium Perfluorooctane Sulfonate Mixed-Surfactant Lamellar Solution. *Colloid Polym. Sci.* **2003**, *281*, 439−446.

(20) Zipfel, J.; Nettesheim, F.; Lindner, P.; Le, T. D.; Olsson, U.; Richtering, W. Cylindrical Intermediates in a Shear-Induced Lamellar-to-Vesicle Transition. *Europhys. Lett.* **2001**, *53*, 335−341.

(21) Le, T. D.; Olsson, U.; Mortensen, K. Packing States of Multilamellar Vesicles in a Nonionic Surfactant System. *Phys. Chem. Chem. Phys.* **2001**, *3*, 1310−1316.

(22) Suganuma, Y.; Imai, M.; Kato, T.; Olsson, U.; Takahashi, T. Order−Disorder Transition of Nonionic Onions under Shear Flow. *Langmuir* **2010**, *26*, 7988−7995.

(23) Nettesheim, F.; Zipfel, J.; Olsson, U.; Renth, F.; Lindner, P.; Richtering, W. Pathway of the Shear-Induced Transition between Planar Lamellae and Multilamellar Vesicles as Studied by Time-Resolved Scattering Techniques. *Langmuir* **2003**, *19*, 3603−3618.

(24) Gentile, L.; Silva, B. F.; Balog, S.; Mortensen, K.; Olsson, U. Structural Transitions Induced by Shear Flow and Temperature Variation in a Nonionic Surfactant/Water System. *J. Colloid Interface Sci.* **2012**, *372*, 32−39.

(25) Gentile, L.; Mortensen, K.; Rossi, C. O.; Olsson, U.; Ranieri, G. A. Multi-Lamellar Vesicle Formation in a Long-Chain Nonionic Surfactant: $C_{16}E_4/D_2O$ System. *J. Colloid Interface Sci.* **2011**, *362*, 1−4.

(26) Medronho, B.; Olsson, U.; Schmidt, C.; Galvosas, P. Transient and Steady-State Shear Banding in a Lamellar Phase as Studied by Rheo-NMR. *Z. Phys. Chem.* **2012**, *226*, 1293−1314.

(27) Oliviero, C.; Coppola, L.; Gianferri, R.; Nicotera, I.; Olsson, U. Dynamic Phase Diagram and Onion Phase Formation in the System $C_{10}E_3/D_2O$. *Colloids Surf., A* **2003**, *228*, 85−90.

(28) Fujii, S.; Richtering, W. Size and Viscoelasticity of Spatially Confined Multilamellar Vesicles. *Eur. Phys. J. E* **2006**, *19*, 139−148.

(29) Ali, A.; Mulley, B. A. Formation of Liquid Crystal and other Non-Fluid Phases in Emulsions Containing Non-Ionic Surfactants. *J. Pharm. Pharmacol.* **1978**, *30*, 205−213.

(30) Strunz, P.; Mortensen, K.; Janssen, S. SANS-II at SINQ: Installation of the former Risø-SANS Facility. *Phys. B* **2004**, *350*, E783−E786.

(31) Mortensen, K.; Almdal, K.; Bates, F. S.; Koppi, K.; Tirell, M.; Nordén, B. Shear Devices for In-Situ Structural Studies of Block-copolymer Melts and Solutions. *Phys. B* **1995**, *213*, 682−684.

(32) Fujii, S.; Richtering, W. Shear Quench-Induced Disintegration of a Nonionic Surfactant $C_{10}E_3$ Onion Phase. *Soft Matter* **2013**, *9*, 5391.

(33) Bergenholtz, J.; Wagner, N. J. Formation of AOT/Brine Multilamellar Vesicles. *Langmuir* **1996**, *12*, 3122−3126.

(34) Roux, D.; Nallet, F.; Diat, O. Rheology of Lyotropic Lamellar Phases. *Europhys. Lett.* **1993**, *24*, 53−58.

(35) van der Linden, E.; Hogervorst, W. T.; Lekkerkerker, H. N. W. Relation between the Size of Lamellar Droplets in Onion Phases and Their Effective Surface Tension. *Langmuir* **1996**, *12*, 3127−3130.

(36) Kosaka, Y.; Ito, M.; Kawabata, Y.; Kato, T. Lamellar-to-Onion Transition with Increasing Temperature under Shear Flow in a Nonionic Surfactant/Water System. *Langmuir* **2010**, *26*, 3835−3842.

(37) Kato, T.; Miyazaki, K.; Kawabata, Y.; Komura, S.; Fujii, M.; Imai, M. Shear-Induced Structural Transition in a Lyotropic Lamellar Phase Studied using Small Angle Neutron and Light Scattering. *J. Phys.: Condens. Matter* **2005**, *17*, S2923−S2928.

(38) Griffith, W. L.; Triolo, R.; Compere, A. L. Analytical Structure function of a Polydisperse Percus-Yevick Fluid with Schulz (gamma) Distributed Diameters. *Phys Rev A.* **1986**, *33*, 2197−220.

(39) Helfrich, W. Lyotropic Lamellar Phases. *J. Phys.: Condens. Matter* **1994**, *6*, A79−A92.

(40) Anderson, D.; Wennerstrom, H.; Olsson, U. Isotropic Bicontinuous Solutions in Surfactant-Solvent Systems: The L3 Phase. *J. Phys. Chem.* **1989**, *93*, 4243−4253.

(41) Würger, A. Bending Elasticity of Surfactant Films: The Role of the Hydrophobic Tails. *Phys. Rev. Lett.* **2000**, *85*, 337−340.

(42) Wheeler, E. K.; Fischer, P.; Fuller, G. G. Flow Instabilities and Shear Induced Phase Transition in Viscoelastic Surfactant Solutions. *J. Non-Newtonian Fluid Mech.* **1998**, *75*, 193−209.

(43) Fardin, M. A.; Ober, T. J.; Grenard, V.; Divoux, T.; Manneville, S.; McKinley, G. H.; Lerouge, S. Interplay between Elastic Instabilities and Shear-Banding: Three Categories of Taylor−Couette Flows and Beyond. *Soft Matter* **2012**, *8*, 10072−10089.

(44) Manneville, S.; Salmon, J. B.; Colin, A. A Spatio-Temporal study of Rheo-Oscillations in a Sheared Lamellar Phase using Ultrasound. *Eur. Phys. J. E* **2004**, *13*, 197−212.

(45) Courbin, L.; Panizza, P.; Salmon, J. B. Observation of Droplet Size Oscillations in a Two- Phase Fluid under Shear Flow. *Phys. Rev. Lett.* **2004**, *92*, 018305.

(46) Angelico, R.; Oliviero Rossi, C.; Ambrosone, L.; Palazzo, G.; Mortensen, K.; Olsson, U. Ordering Fluctuation in a Shear-Banding

Wormlike Micellar System. *Phys. Chem. Chem. Phys.* **2010**, *12*, 8856−8862.
(47) Gentile, L.; Silva, B. F. B.; Lages, S.; Mortensen, K.; Kohlbrecher, J.; Olsson, U. Rheochaos and Flow Instability Phenomena in a Nonionic Lamellar Phase. *Soft Matter* **2013**, *9*, 1133−1140.
(48) Lootens, D.; Van Damme, H.; Hébraud, P. Giant Stress Fluctuations at the Jamming Transition. *Phys. Rev. Lett.* **2003**, *90*, 178301.
(49) Cates, M. E.; Head, D. A.; Ajdari, A. Rheological Chaos in a Scalar Shear-Thickening Model. *Phys. Rev. E* **2002**, *66*, 025202.
(50) Chakrabarti, B.; Das, M.; Dasgupta, C.; Ramaswamy, S.; Sood, A. K. Spatiotemporal Rheochaos in Nematic Hydrodynamics. *Phys. Rev. Lett.* **2004**, *92*, 055501.
(51) Butler, P. Shear Induced Structures and Transformations in Complex Fluids. *Curr. Opin. Colloid Interface Sci.* **1999**, *4*, 214−221.